Utilizing Solar Vapour Energy by Use of Nanofluids in a Direct Absorption Solar Collector

by
Edda Torsdottir Ulset

Master's Program in Energy
with Specialization in Energy Technology

January, 2018

Geophysical Institute
University of Bergen
Norway

Abstract

Traditional solar thermal collectors and photovoltaic (PV) systems suffer from low energy conversion efficiencies. This is mainly due to high thermal losses from overheated absorber plates or solar cells. For steam generation purposes, certain nanofluids (NFs) have been proposed as an alternative due to their high photothermal response and possibility of direct light-to-steam conversion by volumetric absorption. High temperature steam in a direct absorption solar collector (DASC) can potentially be used for electricity generation, purification of drinking water and sterilization. However, efficient and cheap solutions are needed in order to compete against other energy production methods.

Many researchers have focused on the absorption process within NFs, but few have investigated the boiling of NFs creating high temperature steam, especially the effect of varying the nanoparticle (NP) concentration. In this thesis, a low cost solution is proposed by use of carbon black (CB) and iron oxide (IO) NPs, both known to posses high thermal conductivities. Three volumetric absorbers with a variety of concentrations were experimentally investigated and compared with regard to: time to boiling, vapour temperature, evaporation ratio, absorption, and vapour generation efficiency. A surfactant, sodium dodecyl sulfate (SDS), was added to a range of CB NF samples in order to investigate how the dispersion stability effected the boiling. In addition, possible NP contamination of NF condensates were investigated by use of Raman spectroscopy and static light scattering (SLS).

The findings from this study confirm enhanced boiling of CB and IO NFs compared to water, and prove the importance of dispersion stability of NFs. A NP concentration of 2.00 wt.% resulted in the highest performance for all three NFs. The 2.00 wt.% IO NF achieved the highest steam temperature of 129°C and improved the vapour generation efficiency by $88.3 \pm 0.08\%$. The other NFs also presented excellent performance. Nevertheless, the SLS analysis revealed NP contamination in all condensates of CB NF samples containing SDS, in addition to the NF condensates belonging to IO concentrations of $\geqslant 3.00$ wt.%. This can be attributed to the wettability effects of both SDS and increased IO concentration. These findings can prevent the latter concentrations of NFs from being used in applications where clean water is important, or in systems where NP deposition needs to be avoided.

Acknowledgments

Foremost, I would like to express my very great appreciation to my supervisors associate professor Boris V. Balakin of the Department for Mechanical and Marine Engineering at Western Norway University of Applied Sciences, and professor Pawel Kosinski of the Department of Physics and Technology at University of Bergen. Thank you Boris V. Balakin for your passionate participation and valuable input, and thank you Pawel Kosinski for guidance, useful comments and encouragement. They were always very helpful and supportive. My sincere thanks also goes to the entire Solar-Nano[1] research group for constructive comments, in addition to endless meetings and discussions.

A special thanks goes to Chief Engineer Rachid Maad at the Department of Physics and Technology and Department Engineer Roald Langøen at the mechanical workshop for the help in developing the experimental set-up. Thank you Rachid Maad for insightful comments and remarks.

I would also show my gratitude to the bachelor students Sindre Løver Hovden and Mathias Endal Tennebø of the Department for Mechanical and Marine Engineering at Western Norway University of Applied Sciences for their contribution in characterizing the radiative heat flux constituting from the radiation source used for this work. I would also like to thank Chief Engineer Egil Nodland of the Department of Chemistry at the University of Bergen for the chemometric data analysed in this thesis. Furthermore, I thank Irene Heggstad of ElmiLab at the University of Bergen for help and guidance in obtaining electron microscopes data, and Julia Zabednova for programming in ImageJ.

My sincere thanks also goes to Pavel Struchallin from Moscow Engineering Physics Institute for the provision of valuable SDS data of condensate samples obtained in this work. Finally I would like to thank dr Konstantin Redkin and professor Isaac Garcia at Pittsburgh University for their collaboration with the Solar-Nano research group, and especially for the electron microscope characterization of a dried NF sample prepared in this study.

Bergen, January 2018

Edda Torsdottir Ulset

[1] solar-nano.com

Contents

Abstract i

Acknowledgments ii

Nomenclature v

1 Introduction 1
- 1.1 Motivation . . . 1
- 1.2 Specific objectives . . . 4

2 Theoretical Analysis 5
- 2.1 Nanoparticles and nanofluids . . . 5
- 2.2 Literature review . . . 7
- 2.3 Thermal physics . . . 10
  - 2.3.1 Heat transfer . . . 10
  - 2.3.2 Thermal properties of fluids . . . 13
- 2.4 Nanofluid heat transfer . . . 18
  - 2.4.1 Absorption and heat losses . . . 18
  - 2.4.2 Possible boiling scenario . . . 19

3 Methods 21
- 3.1 Study design . . . 21
- 3.2 Nanofluid preparation . . . 21
- 3.3 SEM and TEM characterization . . . 22
- 3.4 Developement of experimental setup . . . 25
  - 3.4.1 Temperature sensors . . . 25
  - 3.4.2 Mass loss measurements . . . 27
  - 3.4.3 Radiation source . . . 27
- 3.5 The experimental set-up . . . 29
- 3.6 Energy conversion . . . 31
  - 3.6.1 Total incident thermal radiation . . . 31
  - 3.6.2 Absorption efficiency . . . 32
  - 3.6.3 Vapour generation efficiency . . . 33

4 Results and discussion 34
- 4.1 Overview . . . 34
- 4.2 Boiling carbon black nanofluids . . . 35
  - 4.2.1 Temperature analysis . . . 37
  - 4.2.2 Mass evaporated . . . 40

4.2.3 Efficiency . . . 42
4.2.4 Summary . . . 45
4.3 Boiling iron oxide nanofluids . . . 46
4.3.1 Temperature measurements . . . 47
4.3.2 Weight measurements . . . 49
4.3.3 Efficiency . . . 51
4.3.4 Summary . . . 54
4.4 Comparing the nanofluids . . . 55
4.5 Characterization of the condensed vapour . . . 58
4.5.1 Overview . . . 58
4.5.2 Raman spectroscopy . . . 58
4.5.3 Static light scattering . . . 62
4.6 Uncertainty analysis . . . 65

5 Conclusion **67**

6 Future work **69**

Bibliography **69**

Appendices **77**

Appendix A Uncertainty calculations **78**

Appendix B Nanofluid boiling graphs I **79**

Appendix C Nanofluid boiling graphs II **87**

Appendix D SEM images **89**

Appendix E Response time **93**

Appendix F Tap water reference data **97**

Appendix G Short communication, submitted to *Applied Thermal Engineering* **98**

Nomenclature

a	Thermal diffusivity	[$m^2 s^{-1}$]
A	Area	[m^2]
A_b	Absorbance	
c	Concentration	[mol m^{-3}]
C_p	Specific heat capacity	[J kg^{-1} K^{-1}]
d	Particle diameter	[m]
E	Energy	[J]
E_{abs}	Absorbed radiation power	[W m^{-2}]
E_v	Emitted radiation power	[W m^{-2}]
g	Gravitational acceleration	[ms^{-2}]
Gr	Grashof number	
h	Heat transfer coefficient	[W m^{-2} K^{-1}]
h_f	Enthalpy of formation	[J kg^{-1}]
h_{fg}	Latent heat of vaporization	[J kg^{-1}]
h_g	Specific enthalpy of saturated vapour	[J kg^{-1}]
h_s	Specific enthalpy of superheated vapour	[J kg^{-1}]
H	Enthalpy	[J]
I	Radiative heat flux	[W m^{-2}]
k	Thermal conductivity	[$Wm^{-1}K^{-1}$]
$K_{a,v}$	Absorption coefficient	[m^{-1}]
L	Characteristic length	[m]
m	Mass	[kg]
$\dot{m}$	Mass flow	[kg s^{-1}]
n	Complex component of the refractive index	
N	Relative complex refractive index (particles to fluid)	
Nu	Nusselt number	
P	Pressure	[Pa]
Pr	Prandl number	
Ra	Rayleigh number	
t	Time	[s]
T	Temperature	[°C, K]
V	Volume	[m^3]
Q	Heat	[J]
$\dot{Q}$	Thermal power	[W]
x, y, z, l	Distance	[m]

Greek letters

α	Absorptivity	
β	Thermal expansion coefficient	[K^{-1}]
δ	Thickness of boundary layer	[m]
η	Efficiency	
ε	Emissivity	
ε_x	Extinction coefficient	[m^2mol^{-1}]
λ	Wavelength	[m]
μ	Absolute viscosity	[kg $m^{-1}s^{-1}$]
ν	Kinematic viscosity	[m^2s^{-1}]
ϕ	Volume fraction	
ρ	Density	[kg m^{-3}]
σ	Stefan-Boltzmann's constant	[W $m^{-2}K^{-4}$]
χ	Particle size parameter	

Subscripts, superscripts

ABS	Absorption
CV	Convection
CO	Conduction
p	Constant pressure

Abbreviations

CB	Carbon black
CNT	Carbon black nanotube
$DASC$	Direct Absorption Solar Collector
GCB	Graphitized carbon black
GNP	Gold nanoparticle
IO	Iron oxide
IR	Infrared
$LCOE$	Levelized cost of energy
$LSPR$	Localized surface plasmon resonance
NF	Nanofluid
NP	Nanoparticle
OAS	One-sun ambient steam generator
PCA	Principal component analysis
PV	Photovoltaic
RT	Response time
SDS	Sodium dodecyl sulfate
SLS	Static light scattering
STE	Solar thermal energy

1. Introduction

1.1 Motivation

In 2016 the world energy consumption was equivalent to $1.544 \cdot 10^{17}$ Wh/year and is estimated to further increase and reach $2.157 \cdot 10^{17}$ Wh/year by the year 2040. Fossil fuels, such as oil, gas or coal, currently cover 85.5 % of the energy use (2016) [1, 2]. In order to prevent emissions to the environment, these need to be replaced with renewable energy. One of the United Nations main goals is to "ensure access to affordable, reliable, sustainable and modern energy for all" [3]. In order to fulfil this target, the utilization of available and clean energy resources must be improved.

The planets most abundant source of energy is the Sun. It emits a thermal power of $3.8 \cdot 10^{26}$ W, where $1.08 \cdot 10^{17}$ W reaches the Earth's surface with an average irradiation of 1366 W/m^2 [4, 5]. The energy potential from the Sun is so immense, that by covering the Earth's surface with solar cells with an efficiency of 0.1, the world energy demand would roughly be covered 420 times. If around 4 % of the area of Sahara desert was covered, the global energy demand would be met. Today the solar energy is utilized by either PV or solar thermal energy (STE) applications. Of the electricity used in 2015, only 1 % was produced by solar energy [1]. For solar energy to be affordable and sustainable, the technological development is crucial. Levelized cost of energy (LCOE)[1] for current solar technologies needs to decrease in order to compete against other conventional energy production methods. Further efficiency enhancement of solar energy technologies could be a key factor to meet future energy requirements.

The energy from the Sun can either be converted directly to electricity by use of PV systems or absorbed in solar thermal collectors for a range of applications. Solar cells can be an appealing choice for energy production, but their construction causes an issue with regard to toxic chemicals, as well as poisonous waste material at the end of their lifetime. PV systems also suffer from overheating, leading to thermal losses and low efficiency. The poor efficiency is mainly due to the bulk materials and dopants lack of ability to absorb the incoming radiation outside of their band gaps. A major reason for selecting a STE application is because they can utilize about twice as much energy as a PV system, see the energy breakdown in figure 1.1. In addition, PV applications lack the capability of storing energy overnight when the Sun is not available. These are important reasons why STE is one of the most promising renewable resources being developed for energy storage, power generation, domestic water heating, distillation, and other industrial processes.

[1] LCOE: a measure of lifetime cost of energy divided by energy production.

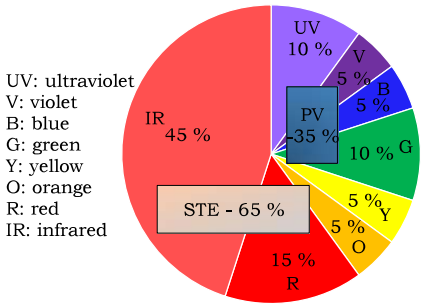

Figure 1.1: Energy breakdown of the solar spectrum. Adapted from Taylor [6].

In addition to the aforementioned applications, STE can potentially be used for water purification purposes. Natural fresh water is scarce in many countries in the world, especially in Africa and the Middle East. Today's available desalination processes of sea water, multi-stage flash distillation and reverse osmosis, require a high electricity demand [7]. Furthermore, these applications are unavailable in areas without electricity. By use of solar heat directly, the energy conversion efficiency will increase and water purification will be independent of available electricity.

To generate electricity a solar collector must achieve high enough evaporation efficiency and steam temperatures to drive a turbine. Conventional power plants rely on large optical concentration of solar energy using mirrors or lenses. This is why solar thermal collectors are usually characterized by their concentration magnitude, divided into two main categories: concentrating collectors and non-concentrating collectors, also called high-temperature and low-temperature solar collectors, respectively [8, 9]. Today the development of existing and new types of solar thermal collectors focuses on minimizing the heat losses within the collector in order to maximize the amount of energy from the available solar radiation.

In concentrated solar collectors, the solar energy heats up a working fluid, for example molten salts or mineral oil, which gives up its energy in a heat exchanger to evaporate a turbine working fluid for electricity production. In most non-concentrating collectors, solar energy is captured by a surface absorber, which heats up the working fluid. Nevertheless, these collectors suffer from high radiative losses due to overheating of the surface. Vacuum can be introduced in some collectors to minimize convectional heat losses, but it is a costly feature when it comes to required material and maintenance. The heat transfer steps for a conventional collector are illustrated in figure 1.2 where R_{CO} represents the energy conversion resistance from the surface absorber to the working fluid.

With advances in technology, concentrated STE power plants are increasing in popularity. The various collectors are classified into four main categories characterized by the way the solar radiation is focused, and the technology used to receive the energy: solar tower, parabolic trough collector, linear Frensel and parabolic dish. The parabolic dish system using a Stirling engine achieves the most efficient energy conversion of all with an efficiency of 18-23% [10]. However, there are several difficulties with current concentrated solar systems: they require a big amount of space and the LCOE is too high compared to other energy applications. In order to reduce the land area and the huge amount of solar concentration needed, a more efficient and cheap energy absorption process is required.

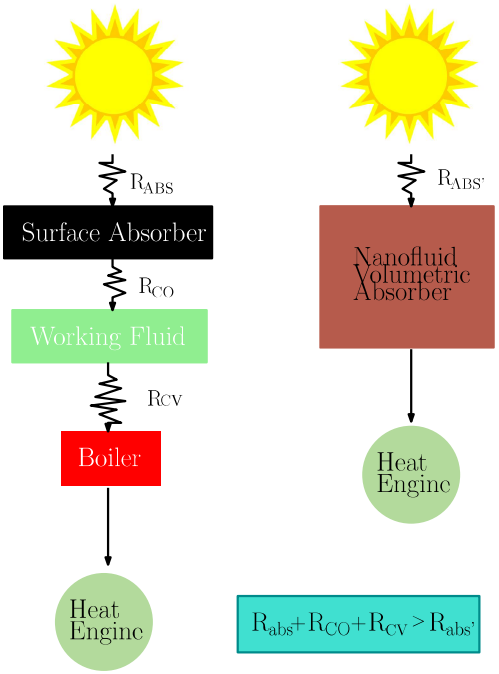

Figure 1.2: Resistance comparison between conventional collector and NF volumetric absorber. R_{ABS}, $R_{ABS'}$, R_{CO} and R_{CV} are thermal resistances corresponding to each heat transfer step.

Recent studies [11–13] have reported 4-40% increased absorption efficiencies by use of NFs in a volumetric absorber, also known as the DASC. NFs, which are by definition NPs dispersed in liquid, hold unique photothermal properties dependent on the type of NPs. The objective is not only to reduce the resistances within the collector, but also to minimize the amount of heat transfer steps achieving a more efficient use of solar energy, see figure 1.2. In addition to power generation, the produced vapour can potentially be used directly in sterilization, distillation, waste water treatment, solar ponds, and in other industrial processes [14–17].

To attain highest possible vapour temperatures with high efficiencies by use of NFs, many factors are involved. The properties of the NF are essential for the vapour generation process. The important factors are the size and shape of the NPs suspended in a liquid (morphology), photothermal properties, rheological behaviour, and dispersion stability [18]. A special attention should be paid to reduce the temperature in the bulk fluid and capture more energy in the superheated parts of the NF [17]. An effort should also be made to use a NF which utilizes the entire solar energy spectrum, that is, wavelengths from 250 to 2500 nm [19], which is one of the objectives of this research.

There is a need of better understanding of the use and behavior of NFs in a direct solar absorber to develop an effective, clean and cheap application to compete against conventional energy production methods. Few researchers have investigated the vapour generation process in NFs by use of solar energy, especially effects of particle concentration [20].

In this thesis three types of NFs are compared experimentally with an extensive variation in concentration to find the optimum NF composition with regard to

absorption and steam generation capabilities. CB and IO NPs were used to produce the NFs due to their enhanced thermal conductivity properties. The effect of adding a surfactant, SDS, to CB NFs was also investigated. Scanning Electron Microscope (SEM) and Transmission Electron Microscope (TEM)-images of the NPs were obtained by use of electron microscopes in order to explore the size distribution and the morphology of the NPs. The condensed steam was captured and analysed by use of Raman spectroscopy to examine if the NPs contaminate the vapour.

1.2 Specific objectives

The specific objectives of this thesis were to:

(i) Optimize and finish an experimental lab set-up.

(ii) Investigate the procedure of producing CB and IO NFs when it comes to chemical additives and concentration.

(iii) Verify NP sizes by use of TEM and SEM analysis.

(iv) Compare CB and IO NFs and concentrations of these with regard to boiling, focusing on:

- Mass change
- Fluid and vapour temperature
- Efficiency

(v) Examine if the NPs contaminate the generated vapour using Raman spectroscopy.

2. Theoretical Analysis

This chapter presents the necessary theoretical background on which the framework of the experimental set-up and the concept of a DASC is based on.

In the first section an introduction on the subject of NPs and NFs is shown. The following section contains a brief literature review of recent studies on NFs illuminated either by a solar simulator, a laser, or directly by the Sun. Next, the attention is directed to the basics of thermal physics in order to elucidate the heat transfer and the approach to calculate the efficiencies of the process. In the same section, further theory on thermal properties relevant for NFs is introduced. Finally, the heat transfer within NFs and potential vapour generation mechanisms are shown.

2.1 Nanoparticles and nanofluids

NPs are particles with a diameter normally between 5 and 100 nm [21]. When these particles are dispersed in a liquid, the fluid is called a NF. For solar heating purposes, some NPs have been studied more than others due to their high photothermal response. It is proven that NP-additions can increase thermal conductivity of bulk fluids used as a heat transfer medium [14, 16, 22]. Some researchers have synthesized and combined custom NPs to enhance their unique heat transfer capabilities [18, 23, 24]. Frequently studied carbon based NPs for heat transfer fluids are CB, graphene, graphitized carbon and carbon nanotubes. Metallic NPs of interest within heat transfer are, for instance, aluminium oxide (Al_2O_3), copper (Cu), gold (Au), IO (Fe_3O_4), nickel (Ni), and titanium oxide (TiO_2).

In addition to demonstrate high thermal conductivity, metallic NPs exhibit exceptional absorption properties due to an optical phenomenon known as localized surface plasmon resonance (LSPR) [17, 25]. When the metallic NPs are illuminated by light consisting of wavelengths larger than the NP size, the electrons located in the conduction band interact with the radiation and cause energetic oscillations, see illustration in figure 2.1. This leads to a rapid temperature increase of the NPs. In addition to material and size, the LSPR frequency is dependent upon factors such as agglomeration (NP clustering), inter-particle distance, and particle shape [26].

NFs have shown to hold different characteristics than fluids containing larger particles (μm or mm) [27]. The decreased particle size leads to a larger surface-to-volume ratio, which improves thermal properties. In addition, nanosized particles do not block channels in which NFs are transported as easily as bigger sized particles [22]. The latter is applicable if the NF were to be transported in tubes, for example in

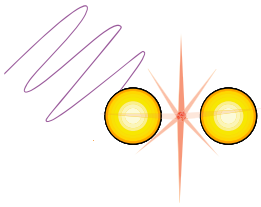

Figure 2.1: LSPR

a circulation system. To avoid blockage of channels, it is also essential that the NPs do not agglomerate. The particle size is therefore important in terms of the overall efficiency of a DASC system. Illumination of these NPs will therefore lead to high temperatures, making them suitable for absorbing radiation from directed sunlight.

CB NPs are one of few substances with similar absorption characteristics as the ideal concept of a black body, which in theory absorbs all incident radiation. Duffie et al. [28] report that 99% of incoming radiation can be absorbed by a thick layer of CB, which makes these NP suited for use in a volumetric absorber. Han et al. [29] also reveal good absorption in the entire solar spectrum for CB NFs. Although the cost of carbon based NPs is lower than of metal NPs [30], the unique nature of ferromagnetic NPs in a NF can be used to be manipulate the heat transfer process by use of magnetic fields.

As mentioned in previous section (2.4.2), NF heat transfer is a complex topic which today's researchers are attempting to understand in full detail in order to find and control the optimum NP material with regard to size, shape and concentration in a bulk fluid. Taylor et al. [19] describes the drawback of having too concentrated NF: absorption will only happen at the surface and light will not penetrate the liquid, which increases heat loss to surroundings. If the concentration is too low, the light will be transmitted and not utilized.

The preparation of NFs are normally categorized into either a one-step or two-step process [19]. In the one-step process, the NPs are directly synthesized inside the base fluid to accomplish the desired volume or mass fraction. This procedure can minimize particle clustering and does not require the additional effort of drying, transportation, and storage of NPs. The drawback with this method is that impurities will exist in the NF due to incomplete reactions inside the NF [27]. The two-step process first involves synthesizing the NPs to a desired shape and size, then adding it to the base fluid. Due to the existing NP production techniques, which are already scaled up in the process industry, the two-step method is more commonly used than the one-step process [31]. However, a big drawback with the two-step process is easily agglomerated NP powders. Although the resulting product from the two-step process will lead to a cleaner result with regard to impurities, the entire process is more energy consuming. This is an important topic when it comes to LCOE of a DASC system.

As a result of the large surface-to-volume ratio of the NPs, the reactive interface increases. NPs tend to agglomerate at a certain distance due to the van der Waals forces [32]. Factors increasing NP clustering are mainly fluid motion, gravitational force and the Brownian motion. In order to prevent agglomeration in NFs, the

solution can either be mechanically stirred using a magnetic stirrer, treated in a high-pressure homogenizer, or dispersed by use of an ultrasonic cleaner or disruptor. Hwang et al. [33] experimentally tested the latter methods using 0.5 wt.% CB NF, with an addition of surfactant (1.0 wt.% SDS) that prevents agglomeration and produces a more stable solution. TEM images from the results showed no improvement using a stirrer, but agglomeration decreased using both an ultrasonic bath and a disruptor. The most stable NF was prepared using the high-pressure homogenizer, which breaks agglomerates in an environment with a high shear force and cavitation.

In order to obtain a stable NF, chemical additions such as surfactants and pH buffers are normally used [33]. However, NFs containing surfactants tend to break down at high temperatures, which will decrease the stability after a certain time [19]. To maintain the NF stability in a DASC, one may suggest adding a sonificator, but this can be complex as well as costly.

2.2 Literature review

The most recent research concerning volumetric absorbers for steam generation purposes is reviewed below. The literature survey presents different approaches of NF production and the utilization opportunities existing for volumetric solar absorbers.

Gold NPs (GNPs) have shown to improve the heat generation within volumetric absorbers. Neumann et al. [23] developed nanoshell particles consisting of silica and gold (SiO_2/Au). They performed experiments showing boiling by illumination of sunlight, generating steam temperatures up to 150°C. The results showed that 80% of the solar energy was converted into steam. This steam could be sufficient enough to drive a turbine or to sterilize medical instruments. Neumann et al. also discovered that by use of nanoshell-particles, the distillation fractions exceeded the azeotropic limit for conventional fractional distillation. An ethanol fraction of 99% was produced, which is much higher than the conventional 95% [21]. Neumann et al. suggest that the nanoshells weakens the hydrogen-bonds between water and pure ethanol, and that this could be an explanation for the high fraction of ethanol [16].

Jin et al. [17] observed an enhanced heating and vapour production using customized GNPs. The results showed NF stability for more than two months with no change in the chemical properties of the NF. The experiments were conducted with focused natural sunlight using Frensel lenses. The GNP NF was placed in an inner tube inside a quartz-tube (to sustain high temperatures), where the tubes were separated by vacuum to reduce heat losses. With an illumination of 220 sun (1 sun = 1000 W/m^2), the highest solar vapour efficiency was 80.3% using 12.75 ppm GNP. Three separate thermocouples were used, unlike in the experiments performed by Neumann et al., where they only used a single measurement point. Jin et al. state that their experimental and numerical data are in significant disagreement with the hypothesised local vapour bubble mechanism elaborated in a later section of the thesis. They report that this mechanism is not possible for low heat fluxes below 1 MW/m^2 produced by concentrated sunlight using e.g. Frensel lenses. However, Jin

et al. claim that this mechanism can occur using high fluence lasers with a radiance higher than 1000 MW/m^2 [17, 34].

An alternative to the costly gold NPs is proposed in a study by Ghasemi et al. [14]. A thermal conversion efficiency of 85% was achieved using a hydrophilic double layer structure (DLS) made of graphene and carbon NPs with a solar illumination source of 10 sun. The DLS transported water through the pores using capillary forces and evaporated the water inside the layer. The carbon foam was used for insulation with graphene on top to absorb the incoming sunlight. For comparison Ghasemi et al. conducted another experiment using CB NF instead of DLS in the same set-up. The NF was made of 0.5 wt.% CB dissolved in deionized water and sonificated for one hour [14]. Using a solar simulator, the results showed higher steam temperatures, faster evaporation and higher efficiency for the DLS. With 10 sun, the vapour and efficiency of the system using CB NF was 80°C and $75 \pm 3\%$. Corresponding data for DLS was 100°C and $85 \pm 3\%$.

Ni et al. [30] investigated graphitized CB (GCB), graphene and CB NFs by sonificating 0.5 wt.% of the respective NPs in distilled water for one hour without any surfactant. In the experimental set-up, the NFs were isolated using a concentric acrylic tube surrounded by aerogel particles. The particles were situated in a bigger tube and sealed off by acrylic discs on top to reduce heat losses. Using 10 sun, vapour generation efficiency was estimated to 69% for all three NFs. Ni et al. state that higher efficiencies are achievable in a larger set-up due to an increased ratio between the surface and volume. Experiments showed that the transient efficiency of GCB and graphene NFs is 7% better than for the CB NF. By comparing all three NFs, GCB reached steady state fastest.

The different properties corresponding to various NPs can be optimized through chemical design. For instance, NPs can be modified in order to increase their dispersion stability in a fluid. Liu et al. [13] experimentally prepared graphene NPs and compared their performance with unmodified graphene in a DASC. The results showed increased dispersion of modified NPs in the ionic liquid $[HMIM]BF_4$ compared to the unmodified graphene. By use of data from numerical simulations and experiments, Liu et al. present no change in transmittance for the modified graphene after being heated to the boiling point, while the unmodified sample induced 20-80% transmittance. They also reveal a stable receiver efficiency for the unmodified sample of 85-89% after the boiling point, but a 37% decrease in efficiency for the unmodified graphene. Liu et al. attribute this to a possible increase in agglomeration in the unmodified graphene for high temperatures, which shows the importance of dispersion stability within a DASC.

In addition to GNPs and carbon based NPs, magnetic NPs are also promising for photothermal applications. Zeng et al. [35] used floating and experimentally prepared Fe_3O_4/C magnetic particles to absorb the incoming sunlight. The IO was incorporated into carbon in order to make a recyclable product and enhancing its photothermal response. Using a solar simulator, Zeng et al. showed an increased evaporation rate by a factor of 2.3 using 3.5% salt water compared to pure water. They demonstrated a successful recycling of the NPs by use of a magnet with almost no influence on the performance.

Chen et al. [7] modified magnetic microspheres consisting of Fe_3O_4 and MFe_2O_4

(M=Mn, Zn, Co) so that they could form a surface layer on top of the water. Evaporation efficiencies of the magnetic microspheres and IO dispersed in water were compared by irradiating a 200 ml sample from above. The efficiency of the microspheres was 1.7 times higher than of the NF consisting of IO.

Sand NPs were prepared and studied by Manikandan et al. [11] in a DASC using propylene glycol and water as the base fluid. The 2.0 vol.% sand propylen glycol NF showed an improved efficiency of 16.5% compared to the pure base fluid. Due to the low freezing point of propylene glycol, this technology could potentially be used in moderate climates. An advantage of using sand is the low cost and high availability of this silica rich substance.

Recent research has focused on the absorption inside the NFs, but few researchers have investigated in which degree the amount of NPs impact the performance of a volumetric absorber. Wang et al. [20] achieved 46.8% efficiency using $19.04 \cdot 10^{-4}$ vol.% NF made of CB nanotubes (CNTs) and distilled water with a radiation in the range of 1-10 sun. Four concentrations of CNT NFs were experimentally tested. Due to several temperature sensors situated in different layers of the NF, they were able to record localized heating in the top layer of the NF. Findings from this study show that heating of the entire bulk fluid was not required in order to boil the NFs.

NFs can also be used for heat transfer applications without high temperature steam generation. Ni et al. [15] demonstrated a floating solar receiver, a one-sun ambient steam generator (OAS), which evaporates the water surface without concentrated solar light. The main part of the OAS consisted of a thermal insulator made of polystyrene foam, which served to float the whole structure on top of a body of water. Situated on the top of the foam, a cermet coated on copper was used as a selective absorber. Finally, the selective absorber was covered with a transparent layer made of bubble wrap in order to reduce convective heat losses. A cotton wick was inserted through the structure to deliver water from the cold water to the hot absorber using capillary forces. Ni et al. demonstrated the OAS's ability to reach steam temperatures up to 100°C even with interruptions in illuminations due to cloud cover or seasonal variation.

Future work is necessary to find inexpensive and efficient methods to generate high temperature steam without the need of pressurizing the system. Few researchers have investigated the effect of steam generation by recording vapour temperature, especially with respect to a wide range of NF concentrations. In addition, a DASC should include condensate recycling in order to optimize the utilization of waste heat and resources. Very few reports were found regarding the matter of condensate contamination of NPs. The extensive potential of using inexpensive NFs, either CB or IO NPs, in a direct solar absorber lays the ground work of this thesis.

2.3 Thermal physics

2.3.1 Heat transfer

Heat is a form of energy transferred from a continuum to another as a result of temperature difference. The Merriam Webster dictionary defines heat as "the energy associated with the random motions of the molecules, atoms, or smaller structural units of which matter is composed" [36]. The mechanism of heat transfer is usually divided into three main categories: conduction, convection and radiation.

Radiation

Radiation is transfer of energy in the form of electromagnetic waves called photons [37]. These energy packets have been observed to possess both wave and particle characteristics. The energy of a single photon is given by hv, where h is the Planck's constant and v denotes its frequency [38]. The frequency of a photon is given by its wavelength and the speed of light. The radiation frequency categorizes the type of radiation (eg. radio waves, microwaves, x-rays, ultraviolet light and gamma rays), where visible light is only a minor part of the electromagnetic spectrum, see figure 2.2. Unlike conduction and convection, heat transfer through radiation does not require a medium and can travel through vacuum or any transparent solid or fluid.

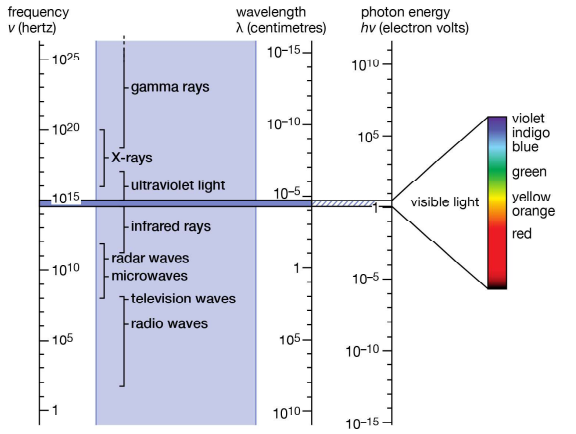

Figure 2.2: Electromagnetic spectrum of light. Reproduced from Encyclopædia Britannica [39].

All bodies with a temperature greater than 0 K emit electromagnetic energy in form of thermal radiation [28]. This is due to intermolecular kinetic energy. Thermal radiation emitted by a body may be calculated using the Stefan-Boltzmann's law: $\dot{Q}_{emit} = \varepsilon\,\sigma\,A\,T_s^4$, where T_s is the temperature [K] of the surface A, ε is the emissivity and σ is the Stefan-Boltzmann's constant: 5.6704×10^{-8} W/(m^2·K^4) [37]. For an idealized surface called a black body, $\varepsilon = 1$. Based on the Stefan-Boltzmann's law, net radiational heat transfer between two surfaces is determined from:

$$\dot{Q}_{1\to2} = \varepsilon\,\sigma\,A_1\,F_{1\to2}\,(T_1^4 - T_2^4), \tag{2.1}$$

where $\dot{Q}_{1\to2}$ is the heat transfer per unit time from body 1 to body 2. A_1 is the surface of body 1. T_1, T_2 are the temperatures [K] of body 1 and body 2, respectively. $F_{1\to2}$ is the view factor, i.e. the fraction of radiation from A_1 falling on A_2.

Incoming radiation can either be absorbed by a body, reflected or transmitted. The fraction of the incoming radiation which is absorbed is given by the absorptivity α of a surface. Like emissivity, absorptivity is a value between 0 and 1, where $\alpha = 1$ for a black body which absorbs all incoming radiation. The amount of energy absorbed by a surface is determined by the wavelength and the temperature of the incoming radiation. The visible, ultraviolet, and near-infra red region of light are of the most dominant wavelengths within solar energy: 0.29-25.00 μm [28]. Photons with short wavelength and high frequency are the ones with the largest energy content. To maximize solar energy utilization an absorber must have excellent absorptivity properties close to 1 without reflecting or transmitting radiation.

Convection

Convection is a heat transfer mechanism occurring between a material and the adjacent liquid or gas, combining conduction and fluid motion. The main types are natural and forced convection. Forced convection is a heat transfer in which a fluid is forced to move. This is usually done to optimize the heat transfer, for example in a heat exchanger. Natural convection is independent of any external source and the fluid motion is due to density gradients only.

The convective heat flux is normally proportional to the difference between the fluid and surface temperature, see figure 2.3 and Newton's law of cooling [40, 41]:

$$\dot{Q}_{conv} = h_c A\,(T_s - T_\infty), \tag{2.2}$$

where T_s is the surface temperature [K], T_∞ is the fluid temperature [K] far from the surface, and h_c is the convective heat transfer coefficient. This coefficient can be found by calculating the average Nusselt number given by $Nu = h_c\,L/k$, where L is the characteristic length and k is the thermal conductivity of the material.

If the temperature of the surface, T_s, has a higher temperature than the ambient temperature, T_∞, the air close to the surface is heated. Due to this heating, the air expands and moves upward, see figure 2.3a. A thermal convective boundary layer will be formed. On the other hand, if the surface is colder than the surrounding fluid, the boundary layer will be mirrored, see figure 2.3b.

The thickness of the boundary layer, δ, can be determined by using thermodynamic calculations involving dimensionless groups such as the Prandtl number and the Grashof number. In order to do this, the following properties of the boundary layer are required: film temperature, volumetric expansion coefficient, and kinematic viscosity.

The Prandtl number represents thermal properties of the fluid and is often extracted from tables [42]. Typical values for the Prandtl number at 1 atm and 20°C are

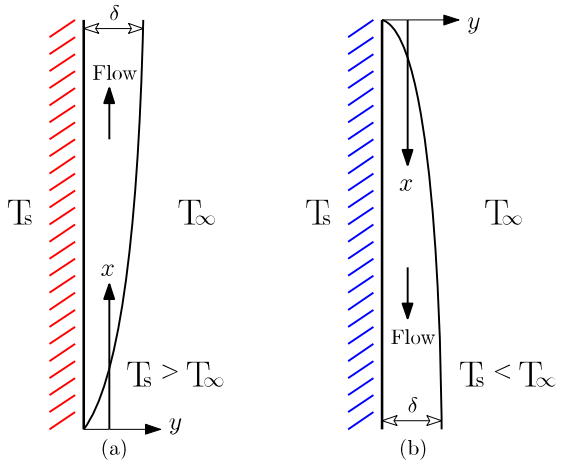

Figure 2.3: Natural convective boundary layers on a vertical surface.

approximately 0.7 for air and 7 for water. By definition, the Prandtl number is given by [42–44]:

$$Pr = \frac{\mu C_p}{k}, \tag{2.3}$$

where μ is the absolute viscosity and C_p is the specific heat capacity of the fluid. For vertical flat plates, the local Grashof number Gr_x for gases is [44, 45]:

$$Gr_x = \frac{g\,\beta\,(T_s - T_\infty)\,x^3}{v^2}, \tag{2.4}$$

where x is the length of the boundary layer and g is gravitational acceleration. The coefficient of thermal expansion β is a property of the fluid. For ideal gases, the coefficient is the inverse of the mean film temperature[1] [40]. Kinematic viscosity ν is given by $\nu = \mu/\rho$, where ρ is the density of the fluid [40]. According to Graebel [44] and Lienhard [42], the thermal boundary layer thickness δ of a vertical isothermal plate is found by:

$$\delta = 3.936\,x \left(\frac{0.952 + Pr}{Pr^2}\right)^{1/4} Gr_x^{-1/4}. \tag{2.5}$$

As mentioned, the film coefficient h_c can be found by calculating the Nusselt number. Nu can be expressed as a function of either the Reynolds or Grashof number, depending on the type of convection analysis. For free convection from a vertical plate, the Nusselt number is given by $f(Gr, Pr)$ [46]:

$$Nu = \left(0.825 + \frac{0.387 Ra^{1/6}}{(1 + (0.492/Pr)^{9/16})^{8/27}}\right)^2, \tag{2.6}$$

where Ra is the Rayleigh number given by $Ra = Pr\,Gr$.

[1]Film temperature: an approximation of the temperature inside the boundary layer, calculated by the mean value of the surface and the fluid temperature.

Conduction

Conduction is transfer of heat through matter due to molecular collisions where more energetic molecules exchange energy with less energetic molecules. Conduction can take place in all phases of matter, but is most significant in solids. The rate of heat transfer in all spatial directions x, y, and z is given by the Fourier's law of heat conduction [40]:

$$\frac{dq}{dA} = -k\left(\frac{\delta T}{\delta x} + \frac{\delta T}{\delta y} + \frac{\delta T}{\delta z}\right) = -k\nabla T, \tag{2.7}$$

where the heat flux dq/dA is proportional to the temperature gradient, ∇T. Eq. (2.7) applies for an isentropic process only, which is an idealized thermodynamic process where the entropy of the system remains constant.

2.3.2 Thermal properties of fluids

Specific heat capacity and latent heat of vaporization

Enthalpy, H, is a thermodynamic state function defined by the sum of the internal energy and the product of pressure and volume: $H = E + PV$, where E is the total internal energy, P the pressure and V the volume of the thermodynamic system [47]. According to the first law of thermodynamics, the change in internal energy is equal to the work done by the system or the energy transferred to the system [48].

When the temperature of a closed system increases, molecular interactions escalate and causes a rise in internal energy. Specific heat capacity is the ratio of change in enthalpy to the change in temperature in a closed system with constant pressure: $C_p = (\Delta H/\Delta T)_p$ [37]. The change in enthalpy of 1 kg of a substance from its constituent elements at its most stable state is conventionally defined as: $h_f = C_p\Delta T$, where h_f is standard enthalpy of formation [49]. In figure 2.4, h_f is given by the energy required to heat one unit mass of water from 0°C to 100°C.

The amount of energy absorbed or released by a material during a phase change without changing its temperature is called latent heat [50]. The energy needed to change the physical state of a substance from liquid to a gas equals the work required to break the intermolecular forces between molecules. This energy is called enthalpy of vaporization or latent heat of vaporization. The heat added to a liquid in order to generate vapour is given by $Q = h_{fg}\Delta m$, where h_{fg} is latent heat and Δm is mass evaporated. The total specific enthalpy of saturated vapour is therefore equal to $h_g = h_f + h_{fg}$.

In figure 2.4, h_s represents specific enthalpy of superheated vapour and is given by $h_s = h_g + C_{ps}(T_s - T_f)$, where T_s is the temperature of the vapour, T_f is the saturation temperature and C_{ps} is the specific heat capacity of the vapour [51].

The values of latent heat of vaporization and specific heat capacity of a substance are often used at standard pressure and temperature (1 atm, 25°C). However, these variables are both pressure and temperature dependent. Figure 2.5 shows how the

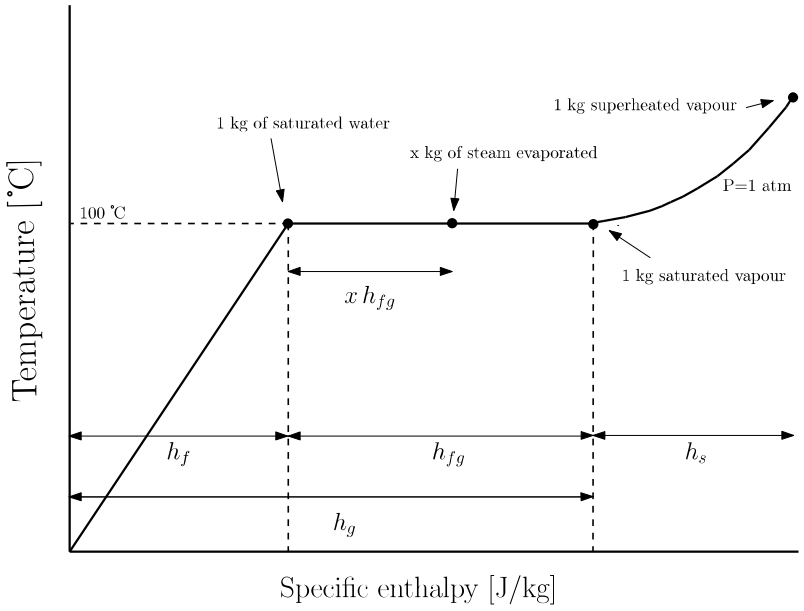

Figure 2.4: Specific enthalpy of water at standard atmospheric pressure.

specific heat capacity of liquid water varies with temperature at 1 atm. The specific heat capacity of liquid water is more or less stable at temperatures from 1°C to 99°C, but a severe decrease in specific heat capacity is observed close to the boiling point. At standard conditions, the specific heat capacity of water is 4180 J/(kg·K), the specific heat capacity of vapour is 1860 J/(kg·K), and the latent heat of vaporization of water is 2257 kJ/kg [20].

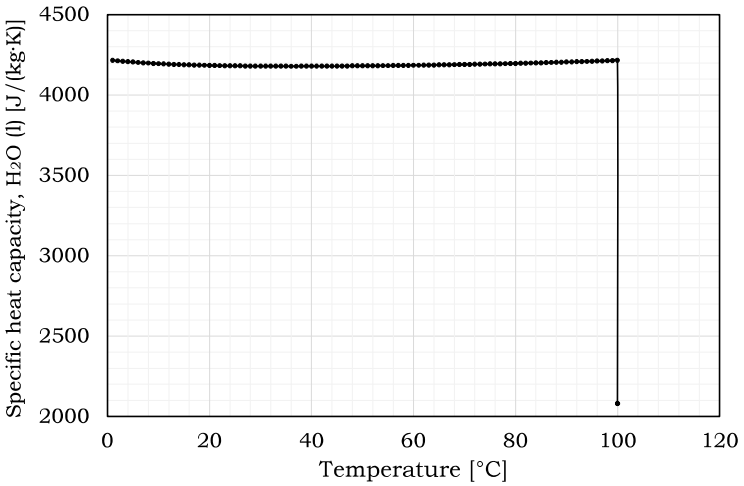

Figure 2.5: Heat capacities of water at standard atmospheric pressure [52].

It has been reported that presence of NPs in water possibly enhances the specific heat capacity and latent heat of vaporization [53–55]. Chieruzzi et al. [56] reported an increase of C_p for $NaNO_3$-KNO_3 NFs containing SiO_2/Al_2O_3 NPs. Ameen et al. [55] revealed trends showing higher h_{fg} values by increased volume fractions and decreased NP sizes, both in an experimental study and through molecular dynamic simulations. They also reviewed the possibility that the increase could be caused by extra bonds between the NPs and the water molecules. Chen et al. [54] reported reduced effects on h_{fg} by adding a surfactant to distilled water droplets. A smaller value of h_{fg} will

enhance water evaporation, while a larger h_{fg} requires additional energy for inducing a phase change. It should be noted that few researchers have investigated the NP effect on C_p and h_{fg}, so this topic is still not explored thoroughly.

Thermal conductivity

Thermal conductivity is a property describing the heat transfer capability of a given material, denoted as k. All materials conduct heat differently, depending on its chemical composition and temperature. The thermal conductivity of a solid, liquid, or gas is related to the specific heat capacity by $k = a\,\rho\,C_p$, where a is thermal diffusivity [57].

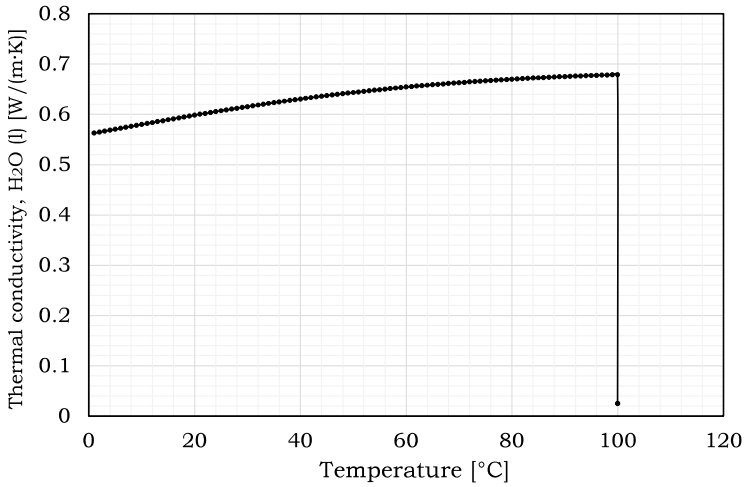

Figure 2.6: Thermal conductivity of water at standard atmospheric pressure [52].

Figure 2.6 illustrates how the thermal conductivity of water varies with temperature at constant pressure. Although water exhibits a high heat capacity, the thermal conductivity of water is rather in the mid-range compared to other substances.

As mentioned in section 2.1, additions of NPs can enhance the thermal conductivity of NFs. Table 2.1 presents thermal conductivity of common materials, which could potentially be used in a NF. Several reports show that NPs exhibiting high values of k increase the thermal conductivity of the bulk fluid [22]. For instance, a thermal conductivity study by Wang et al. [58] showed up to 15% k-enhancement for the water based Al_2O_3 NF and 18% for the water based Cu NF by use of 0.8 wt.% NPs. The higher k-values for the Cu NFs are attributed to the high thermal conductivity of Cu, see table 2.1.

However, some reports conclude that the k of certain NPs does not directly correlate to the k of a NF [22]. For instance, even though Al_2O_3 crystals have a higher thermal conductivity than TiO_3, a study by Yoo et al. [59] revealed a 14% higher k-value for the TiO_3 NF compared to water and only a 4% increase in thermal conductivity for the Al_2O_3 NF. They concluded that that the most important factor determining the thermal conductivity of a NF is the surface-to-volume ratio of the NPs. By comparing water based IO NPs with other water based NFs, the same effect is seen. Zhang et al. [60] discovered 38% k-enhancement for 4.0 vol.% IO NF and 30% higher k for NFs containing Al_2O_3 or TiO_3. Jamilapanah et al. [61] investigated the thermal

conductivity in a range of IO concentrations in ethylene glycol. Their results present an increased thermal conductivity of 51.8% compared to the bulk fluid, by use of 2.00 wt.% IO.

Although many researchers have experimentally investigated the possible increased thermal conductivity of NFs, a robust physical theory explaining the enhancement has not yet been proposed [57].

Table 2.1: Thermal conductivity of materials in room temperature [62–65]. Units are W/(m·K).

Material	k	**Material**	k	**Material**	k
Carbon nanotube	2000	Graphite	167.4	MgO	59.6
SiC	490	Si	160	Al_2O_3	27
Ag	430	Mg	156	Ti	20.9
Cu	400	Zn	111.7	CuO	18
AlN	350	Ni	87.7	TiO_2	6.7
Gold	318	Fe	80.3	Fe_2O_3	0.58
Al	226	ZnO	60	CB	0.375

Absorbance

In chemistry, absorbance is the logarithmic relationship between the incident radiative heat flux to the transmitted radiative heat flux through a material [66]. Absorbance differs from absorptivity (mentioned in subsection 2.3.1) because it also includes reflection and scattering phenomena occuring in a medium. The absorbance of a medium is found using the Beer-Lambert's law [67]:

$$A_b = \log\frac{I_0}{I} = \varepsilon_x \, l \, c, \tag{2.8}$$

where I_0 denotes the incoming radiative heat flux, I denotes the transmitted radiative heat flux, c is the molar concentration, l is the coordinate along the length direction, and ε_x is the molar absorptivity also called the extinction coefficient. Eq. (2.8) states that the absorbance of a liquid is proportional to its concentration. The Beer-Lambert's law can also be simplified by introducing the absorption coefficient: $K_{a,v} = \varepsilon_x \, c$, which is dependent upon the wavelength of the incident light and the material or fluid absorbing the radiation.

In order to attain the absorbance of a medium, the extinction coefficient must be found. The extinction coefficient of a fluid, ε_x, is given by [57]:

$$\varepsilon_x = \frac{4\pi n}{\lambda}. \tag{2.9}$$

In Eq. (2.9), λ is the wavelength of the incident light and n is the complex refractive index, which is an optical property that can be found in many handbooks, for example Palik [68].

If the fluid contains particles, the extinction coefficient can be difficult to find if it is a strong scattering medium [19]. This is typical for high concentrations of particles. Mie scattering theory is a collection of physical laws describing the scattering regime of independent particles [19, 57]. The theory was originally derived for spheres, but was later developed for irregularly shaped particles. The extinction coefficient of a fluid containing particles can be assumed to be found through a simple addition of the extinction coefficients corresponding to each phase [19]:

$$\varepsilon_x = \varepsilon_{x,p} + \varepsilon_{x,bf}, \tag{2.10}$$

where $\varepsilon_{x,p}$ is the extinction coefficient of the particles and $\varepsilon_{x,bf}$ denotes the extinction coefficient of the base fluid given by Eq. (2.9).

Since a major part of the incident light consists of wavelengths with a magnitude larger than the sizes of commonly used NPs (5-100 nm), the scattering (Q_{scat}), absorption (Q_{abs}) and extinction (Q_{ext}) efficiencies for individual NPs can be found [19,57]:

$$Q_{ext} = Q_{abs} + Q_{scat}. \tag{2.11}$$

The absorption and scattering efficiencies are obtained by use of equations according to the Mie scattering theory [19,57], and are not shown in this thesis. These equations involve the particle size parameter χ in addition to the relative complex refractive index N. The latter property describes scattering from particles to the fluid and can be found experimentally by use of a refractometer. The particle size parameter χ, also called the relative particle size, is given by $\chi = \pi d/\lambda$, where d is the mean particle diameter.

Since the scattering efficiency is proportional to d^4 [19, 57], Q_{scat} can be neglected when $Q_{abs} >> Q_{scat}$. This only applies if the NPs and any agglomerates formed in the solution are small. In this case, the extinction coefficient of the particles can be calculated by the approximation:

$$\varepsilon_{x,p} = \frac{300\phi(Q_{abs} + Q_{scat})}{2d} \approx \frac{300\phi Q_{abs}}{2d}, \tag{2.12}$$

where ϕ is the volume fraction of NPs in the bulk fluid [19]. The scattering efficiencies are based on a completely transparent base fluid. This is not true for water, which efficiently absorbs infrared radiation. The absorption of the bulk fluid is taken into account in Eq. (2.10) in order to find the extinction coefficient of the NF.

2.4 Nanofluid heat transfer

2.4.1 Absorption and heat losses

One of the main challenges with all kind of solar energy systems is reduction of heat losses to surroundings. In order to maximize the efficiency of solar thermal systems, it is essential to understand the heat transfer in both conventional surface absorber systems and DASCs.

When radiation passes through matter, the energy from the photons may be absorbed. The magnitude of absorption depends on the characteristics and the length of the material. In surface absorber systems the absorbed radiation is $E_{abs} = \alpha \cdot I_0$, see figure 2.7a. For volumetric absorbers the absorptivity of a NF depends both on the material and the thickness of the fluid layer y [69]. The energy absorbed in a volumetric absorber can be found by rearranging Beer-Lambert's law, Eq. (2.8), by use of $E_{abs} = I_0 - I$:

$$E_{abs} = I_0 \left[1 - \exp(-K_{a,v}\, y)\right], \tag{2.13}$$

where $K_{a,v}$ is the absorption coefficient and y is the thickness of the fluid layer illustrated in figure 2.7b.

Due to particle settling, convection, profile non-uniformity, agglomeration, and other phenomena such as chemical polarity, a fluid can hold different concentration distributions. This can be illustrated as separate layers within a fluid. For further enhancement of absorption capabilities the NFs can be engineered to consist of various layers holding different absorption properties, see figure 2.7c. Figure 2.7b and c demonstrates the differences between conventional surface absorbers and two types of DASC systems. For a NF consisting of layers with various absorption coefficients $K_{a,n}$ and thicknesses y_n, Eq. (2.13) can be rewritten as [69]:

$$E_{abs} = I_0 \left[1 - \exp(-K_{a,1}y_1 - K_{a,2}y_2 \ldots - K_{a,n}y_n - K_{a,n-1}y_{n-1})\right]. \tag{2.14}$$

Eq. (2.14) demonstrates that by adjusting the thickness layer of the NF and its concentration, the most effective absorption configuration can be found. If the NF is made of magnetic NPs, their position could potentially be controlled using magnets.

As mentioned in the radiation section 2.3.1, all bodies with a temperature higher than absolute zero emit thermal radiation. The radiative losses depend on the total hemisphere from which the radiation is emitted. For surface absorbers the total hemisphere consists of a half of the hemisphere of a volumetric absorber, see figure 2.7. By use of the Kirchhoff's radiation law, which states that an idealized black body in thermal equilibrium emits the same amount of energy being absorbed, $\alpha = \varepsilon$, the radiative losses from a volumetric absorber, consisting of one layer, can be calculated combined with the Stefan-Boltzmann's law [69, 70]:

$$E_v = \left[1 - \exp(-K_{a,v}\, y)\right]\sigma T_v^4, \tag{2.15}$$